PHYSICAL REVIEW B **74**, 020101(R) (2006)

# Investigation on the origin of the magnetic moment of $BiFeO_3$ thin films by advanced x-ray characterizations

Hélène Béa,[1] Manuel Bibes,[2,*] Stéphane Fusil,[1] Karim Bouzehouane,[1] Eric Jacquet,[1] Karsten Rode,[1,†] Peter Bencok,[3] and Agnès Barthélémy[1]

[1]*Unité Mixte de Physique CNRS/Thales, Route Départementale 128, 91767 Palaiseau, France*

[2]*Institut d'Electronique Fondamentale, Université Paris-Sud, 91405 Orsay, France*

[3]*European Synchrotron Radiation Facility, 38043 Grenoble Cedex, France*

(Received 13 April 2006; published 17 July 2006)

Single phase (001)-oriented $BiFeO_3$ (BFO) thin films grown by pulsed laser deposition can only be obtained in a narrow window of deposition pressure and temperature and have a low magnetic moment. Out of the stability window Fe- or Bi-rich impurity phases form, which has a strong impact on the physical and structural properties of the films, even for impurity concentrations hardly detectable by standard x-ray diffraction measurements. By using more sensitive tools such as x-ray absorption spectroscopy and x-ray magnetic circular dichroism and performing advanced x-ray diffraction characterization, we show that in nonoptimal conditions Fe forms ferrimagnetic $\gamma$-$Fe_2O_3$ precipitates that are responsible for virtually all the ferromagnetic signal measured on such BFO films by standard magnetometry. This confirms that the BFO phase has a very low intrinsic moment that does not depend on strain. We also study the influence of film thickness on the nucleation of parasitic phases and find that epitaxial strain can stabilize the pure BFO phase in slightly overoxidizing growth conditions.

DOI: 10.1103/PhysRevB.74.020101 PACS number(s): 78.70.Dm, 75.50.−y, 75.70.−i

Multiferroic materials display simultaneously several types of order, like ferroelectricity and magnetism.[1,2] Beside their exciting physics, multiferroics could bring solutions for applications in many fields,[3] such as agile electromagnetics, optoelectronics, or spintronics.[4] Indeed, the magnetoelectric coupling existing in multiferroics[2,5] could allow us to reverse magnetization by applying an electric field[6,7] instead of a magnetic field.

To achieve this, a straightforward way would be to use a ferromagnetic layer coupled to a ferromagnetic multiferroic. However, such ferromagnetic multiferroics are extremely rare, a known exception being $BiMnO_3$ (Ref. 1) that has a magnetic Curie point ($T_C$) well below room temperature. In fact, most multiferroics are antiferromagnetic or weak ferromagnets. In this context, the report of a gigantic enhancement of the magnetic moment in $BiFeO_3$ (BFO) thin films compared to bulk[8] was very exciting given the high magnetic transition temperature of this compound (640 K). Yet, some controversy over these results appeared shortly after publication and the intrinsic magnetic properties of $BiFeO_3$ films are still debated.[9,10]

A few months ago, we reported that single-phase BFO films can only be obtained in a rather narrow range of deposition pressure $P_{O_2}$ and temperature.[9] We found that films not showing indications of parasitic Fe-rich phases have a low bulklike magnetic moment ($\sim 0.02\mu_B$/Fe) (Ref. 11) while films containing Fe oxides display a ferromagnetic behavior. Even though this suggests that in these impure films all the ferromagnetic signal comes from the Fe oxides, it is not clear whether the BFO phase in such films could not have some ferromagnetic moment. In this Rapid Communication we have addressed this issue more quantitatively and demonstrate that even in Fe-oxide-rich samples the BFO phase has virtually no magnetic moment, irrespective of its strain state. We also address the influence of strain on the nucleation of extra phases and find that in overoxidizing conditions tending to favor the presence of Bi oxides, strain actually helps to stabilize the BFO phase.

The films were grown by pulsed laser deposition on (001)-oriented $SrTiO_3$ (STO) substrates.[9] In order to study the structure of the films, we performed high-resolution x-ray diffraction (XRD) using a Panalytical X'pert PRO equipped with a Ge (220) monochromator. Magnetization loops were measured at 10 K with the magnetic field oriented in-plane using a superconducting quantum interference device (SQUID).

X-ray absorption spectroscopy (XAS) and x-ray circular magnetic dichroism (XMCD) were performed at the ID08 line of the European Synchrotron Radiation Facility at the Fe $L_{2,3}$ edges, at 10 K. Both magnetic field (in the range of $\pm 6T$) and propagation vector of photons were perpendicular to the sample surface with a circular polarization of nearly 100%. The spectra were collected in the total electron yield mode that has a typical probing depth of $\sim 50$ Å in oxides.

For this study, we have fixed the deposition temperature to 580 °C and varied $P_{O_2}$ and the deposition time, hence the film thickness ($t$). We then analyzed the influence of pressure and thickness on the onset of parasitic phases via XRD. The proportions of the different phases have been calculated (Table I) and the results are summarized in Fig. 1(a). For $P_{O_2} \leq 10^{-3}$ mbar, Fe oxides are detected in all the films, irrespective of thickness. The diffraction lines for this Fe oxide correspond to those of $\gamma$-$Fe_2O_3$ (maghemite), a ferrimagnetic material with a $T_C$ of $\sim 850$ K and a magnetic moment of $\sim 420$ emu cm$^{-3}$ or $1.25\mu_B$/Fe.[12] At $P_{O_2} = 1.2 \times 10^{-2}$ mbar, we can notice that for $t \leq 70$ nm, no parasitic phases are observed while for $t \geq 120$ nm, $Bi_2O_3$ phases are detected. This suggests different mechanisms for the appearance of Fe- and Bi-rich phases. We will study in the following the influence of these extra phases on the structure and properties of the films.

At this point it is important to recall that all films without

 ©2006 The American Physical Society

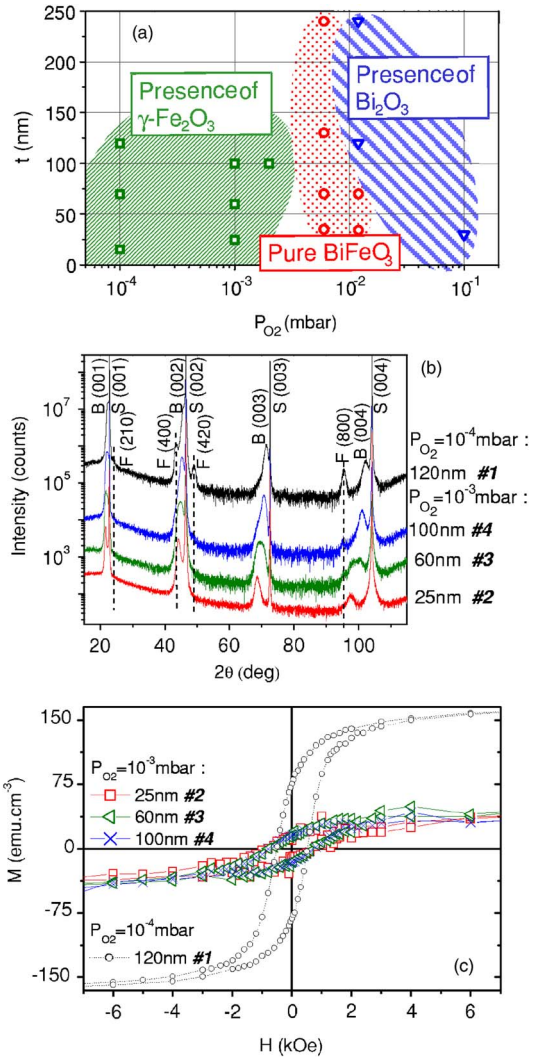


FIG. 1. (Color online) (a) Film composition vs growth pressure and film thickness. (b) XRD diagram of films 1 to 4. *B* stands for BFO peaks, *S* for STO, and *F* for the $\gamma$-$Fe_2O_3$ parasitic phase. The vertical dashed lines show the location of the $\gamma$-$Fe_2O_3$ reflections. (c) SQUID measurements of the same samples ($T$=10 K).

parasitic phases (e.g., films grown at $6\times10^{-3}$ mbar) have very low magnetic moments ($\leq 0.02\mu_B$/Fe).[9] In Fig. 1(b), we show XRD spectra for films (#) 1–4 grown at $10^{-4}$ and $10^{-3}$ mbar. In addition to the (00$l$) peaks due to STO and BFO, several peaks corresponding to $\gamma$-$Fe_2O_3$ reflections are detected. This is particularly clear for film 1. At $10^{-3}$ mbar only the (800) peak of $\gamma$-$Fe_2O_3$ is visible but lies on the edge of the BFO (004) peak. This parasitic phase is thus not easily detectable by XRD and from these data it is not possible to conclude on the presence or absence of $\gamma$-$Fe_2O_3$ in the thinner film. We also note that for the $10^{-3}$ mbar series, the position of the BFO peaks varies due to strain relaxation occurring upon increasing $t$.

Figure 1(c) shows magnetization hysteresis cycles $M(H)$ for these four films. Remarkably, the three samples grown at $P_{O_2}=10^{-3}$ mbar show the same volumic magnetic moment. For film 1, the volumic magnetic moment is larger, which also corresponds to a larger proportion of $\gamma$-$Fe_2O_3$ as detected by XRD.

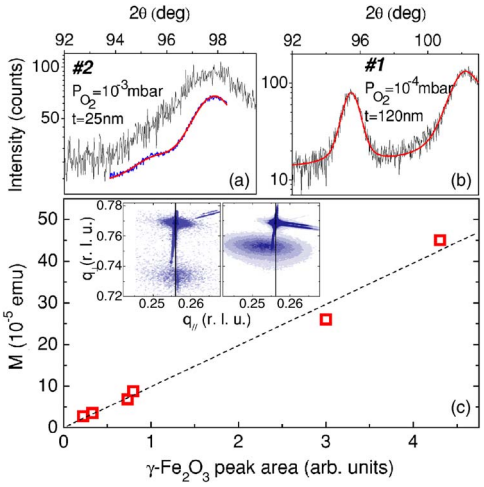


FIG. 2. (Color online) (a) XRD pattern in the 92°–100° $2\theta$ range of film 2. The upper spectrum is a zoom of Fig. 1(b). The lower one is a pattern measured with a higher counting rate (see text). The bold line is a fit of the (004) BFO and (800) $\gamma$-$Fe_2O_3$ peaks. (b) Zoom of the XRD pattern of film 1 shown in Fig. 1(b). The bold line is a fit of the BFO and $\gamma$-$Fe_2O_3$ peaks. (c) Saturation magnetization for samples grown at $10^{-3}$ and $10^{-4}$ mbar as a function of the area of the (800) $\gamma$-$Fe_2O_3$ peak. The reciprocal space maps of the (013) reflections reveal a fully strained state for a 25 nm film (left) and a partially relaxed state for a 100 nm film (right), both grown at $10^{-3}$ mbar. r.l.u. stands for reciprocal lattice units.

The observation of a large magnetic moment for film 2 suggests the presence of $\gamma$-$Fe_2O_3$ even though standard XRD could not detect it. To solve this issue we performed additional XRD with much longer counting times in the $2\theta$ =93–98° range so as to increase the signal-to-noise ratio [see Fig. 2(a)]. On this scan, a shoulder is clearly visible at the left of the BFO (004) peak, located at $2\theta\approx95.5°$, i.e., where the (800) reflection of $\gamma$-$Fe_2O_3$ shows up for the thicker films.

To better quantify the relation between the amount of maghemite and the magnetization, we have fitted the XRD spectra in the $2\theta$=90–98° range with three pseudo-Voigt functions corresponding to the (004) BFO peak, the (004) STO peak, and the (800) $\gamma$-$Fe_2O_3$ peak. The STO fit allows the normalization of the area of the $\gamma$-$Fe_2O_3$ peak to that of

TABLE I. Composition of the films in the different growth conditions.

| Film | $P_{O_2}$ (mbar) | $t$ (nm) | BFO (%) | $\gamma$-$Fe_2O_3$ (%) | $Bi_2O_3$ (%) |
|---|---|---|---|---|---|
| 1 | $10^{-4}$ | 120 | 52±1.5 | 48±1.5 | <0.4 |
| 2 | $10^{-3}$ | 25 | 81±2 | 19±2 | <1.7 |
| 3 | $10^{-3}$ | 60 | 79±2 | 21±2 | <0.7 |
| 4 | $10^{-3}$ | 100 | 87±1.5 | 13±1.5 | <0.5 |
| 5 | $6\times10^{-3}$ | 35 | >97.2 | <1.4 | <1.4 |
| 6 | $1.2\times10^{-2}$ | 70 | >98.7 | <0.7 | <0.6 |
| 7 | $1.2\times10^{-2}$ | 120 | 83±2 | <0.4 | 17±2 |
| 8 | $1.2\times10^{-2}$ | 240 | 79±2 | <0.2 | 21±2 |

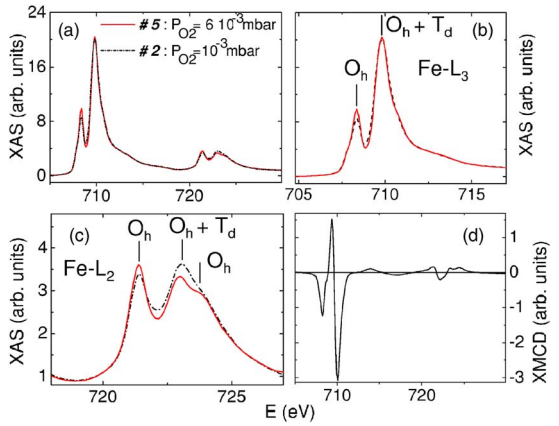


FIG. 3. (Color online) (a) XAS spectra at the Fe $L_{2,3}$ edge for films 2 and 5. (b) and (c) are zooms of (a) next to the $L_3$ and $L_2$ edges respectively. The lines correspond to an attribution of the $Fe^{3+}$ peaks from multiplets calculation (Ref. 18). (d) XMCD of sample 2.

a substrate peak. We thus obtain the area $A$ of the $\gamma$-$Fe_2O_3$ (800) peak, proportional to the volume of $\gamma$-$Fe_2O_3$ present in the film [see an example of such fits in Fig. 2(b)]. As visible in Fig. 2(c), $M$ increases linearly with $A$, which shows that the magnetic signal in these films is proportional to the amount of $\gamma$-$Fe_2O_3$. Of great relevance is the observation that the magnetization extrapolates to zero for $A=0$ thus demonstrating that in these films, virtually *all* the magnetic signal comes from $\gamma$-$Fe_2O_3$. In other words, the BFO phase has a very low magnetization, if any. Reciprocal space mappings collected on the films considered in the above analysis reveal a variety of strain states [see the insets in Fig. 2(c)]. Hence, our observation of a very low moment for the BFO phase in all these films rules out a role of strain in increasing the BFO magnetization for this range of growth pressure and temperature. This is in contrast to what was suggested by Wang *et al.*[8] for higher growth pressure and temperature but in agreement with theoretical predictions[13] and with Eerenstein *et al.*[10]

To get deeper insight on the microscopic magnetic properties of our BFO films, we have performed XAS and XMCD measurements on films 2 and 5. XAS at the $L_{2,3}$ edge of Fe allows the determination of its valence and environment. In pure BFO, Fe is octahedrally coordinated by six oxygen ions and has a valence of 3+. In $\gamma$-$Fe_2O_3$ the iron valence is also 3+, but 5 of the 8 Fe ions contained in a unit cell are in octahedral (Oh) sites while the other 3 are in tetrahedral (Td) sites.[14] In Fig. 3(a), we show XAS spectra for both films. The general shape of the spectra is very similar to that obtained on $LaFeO_3$, a perovskite in which $Fe^{3+}$ ions are in an octahedral environment.[15] A large difference is observed with a XAS spectrum for $Fe_3O_4$ (Refs. 16 and 17) in which 1/3 of the iron ions are in a 2+ state, strongly suggesting that Fe ions have a valence close to 3+ in both films.

A closer look at the XAS data [Figs. 3(b) and 3(c)] allows the identification of several differences between the two films. Especially, the shoulder at the right of the 723 eV peak of the $L_2$ edge, typical of $Fe^{3+}$ in an octahedral environment,[18] is clearly visible for film 5 but less pronounced for film 2. This indicates a substantial amount of $Fe^{3+}$ at Td sites in this latter sample. Consistent with this observation is the lower XAS signal measured at the 721.5 eV peak. We conclude that film 2 has a larger proportion of $Fe^{3+}$ in Td sites, as expected in the presence of $\gamma$-$Fe_2O_3$.

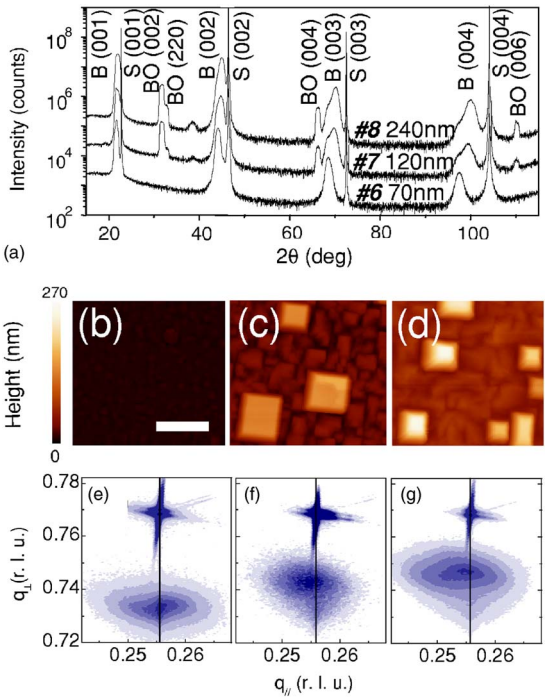


FIG. 4. (Color online) (a) XRD pattern of samples 6, 7, and 8. The peaks are indexed as *B* for BFO, *S* for STO, and *BO* for the extra-phase $Bi_2O_3$. AFM [(b),(c),(d)] and reciprocal space mappings around the (013) direction [(e),(f),(g)] for films 6 [(b) and (e)], 7 [(c) and (f)], and 8 [(d) and (g)]. For the AFM images, the white bar corresponds to 1 $\mu$m.

In film 5 no clear XMCD signal was measured, suggesting a very low magnetic moment, in agreement with SQUID results. On sample 2 we find a large dichroic signal [see Fig. 3(d)], very similar to that of $\gamma$-$Fe_2O_3$.[17,18] More quantitatively, we can calculate the spin moment $M_S$ and the orbital moment $M_L$ using the sum rules, which yields $M_S = 0.22 \pm 0.05 \mu_B$/Fe and $M_L = 0.02 \pm 0.005 \mu_B$/Fe. The total magnetic moment is $M = M_S + M_L = 0.24 \pm 0.06 \mu_B$/Fe, in very good agreement with the magnetization measured by SQUID, 40 emu $cm^{-3}$ or $0.27 \mu_B$/Fe. Since bulk maghemite has a magnetic moment of $1.25 \mu_B$/Fe, the proportion of $\gamma$-$Fe_2O_3$ near the surface (probed by XMCD) is thus close to the 20% calculated for the volume (see Table I). Therefore, the distribution of this extra phase in the film seems to be homogeneous, which is consistent with the presence of $\gamma$-$Fe_2O_3$for all thicknesses, particularly for the lower ones.

We now examine in more detail the high-pressure region of the diagram shown in Fig. 1(a). In Fig. 4(a), XRD spectra of samples grown at $1.2 \times 10^{-2}$ mbar with different thicknesses are shown. For the thinner film, no parasitic phases are observed, even for long counting rates (not shown), while at larger $t$ $Bi_2O_3$ lines show up. On the AFM images of Figs. 4(b)–4(d), we can see that the detection of $Bi_2O_3$ is accompanied by the nucleation of square outgrowths on the surface

for $t \geq 120$ nm. Auger electron spectroscopy confirmed that these hillocks are Bi rich and Fe poor, thus likely corresponding to $Bi_2O_3$ (Ref. 9). When $t$ increases, these outgrowths become higher (as high as the film thickness).

It is interesting to correlate the nucleation of $Bi_2O_3$ with the strain state of the films using reciprocal space maps close to the (013) reflection [see Figs. 4(e)–4(g)]. The relative positions of the STO and BFO peaks indicate a fully strained state for the 70 nm film while they correspond to a partially relaxed state for the 120 and 240 nm films. This correlation between strain relaxation and the nucleation of $Bi_2O_3$ suggests that strain favors the formation of a metastable BFO phase at the expense of the stable $Bi_2O_3$. The stabilization of metastable perovskite phases by strain has indeed been reported by several groups.[19,20] More quantitatively, the formation energy difference $\Delta E$ between the stable and the metastable phase is given by

$$\Delta E = t\left[(\Delta g_S - \Delta g_M) - (\mu/(1-\nu))\epsilon^2\right] + (\sigma_S^I - \sigma_M^I). \quad (1)$$

$\Delta g_S$ and $\Delta g_M$ are the stable and metastable phase formation energies, respectively, $\mu$ and $\nu$ the shear and Poisson coefficients of the metastable phase, $\epsilon$ the strain, and $\sigma_S^I$ and $\sigma_M^I$ the interface energies for the stable and metastable phases, respectively. In principle the first term is always negative. The second term is positive if, for instance, the interface between the metastable phase and the substrate is coherent (i.e., the metastable phase grows in a fully strained state) while the interface between the stable phase and the substrate is not (e.g., if the mismatch between the stable phase and the substrate is large). Thus, when $t$ is small, $\Delta E$ can be positive and the growth of the metastable phase is favored, but there is a critical thickness $t_c$ above which $\Delta E$ becomes negative, which leads to the formation of the stable phase. On the other hand, if the structure of the metastable phase relaxes (hence enhancing its interface energy), the formation of the stable phase can become more favorable for $t < t_c$.

In our case, we have seen that BFO grows fully strained on the STO substrate up to $t \approx 70$ nm so that the BFO/STO interface energy $\sigma_{BFO/STO}$ is low and the conditions for the growth of the metastable BFO phase are met. The formation of $Bi_2O_3$ occurs when BFO relaxes, hence increasing $\sigma_{BFO/STO}$. It is thus tempting to conclude that this relaxation unbalances Eq. (1) and favors the formation of the stable $Bi_2O_3$ phase. However, since many parameters in Eq. (1) are unknown, it is not possible to calculate $t_c$. Thus we cannot be fully conclusive on whether the formation of $Bi_2O_3$ is just related to the thickness increase or directly due to the observed structural relaxation.

In summary, we have found that epitaxial BFO films grown at $6 \times 10^{-3}$ mbar are single-phase for thicknesses up to at least 240 nm. For lower pressures, all the films contain $\gamma$-$Fe_2O_3$, as evidenced by XRD, XAS, and XMCD. We showed that this extra phase is responsible for all the magnetic moment in the film so that, at least in all the range of growth conditions we have explored, the BFO phase has a very low magnetic moment, if any. At $1.2 \times 10^{-2}$ mbar BFO films are also single-phase for $t \leq 70$ nm while $Bi_2O_3$ appears in the film above that thickness. Reciprocal space maps analysis suggests a role of strain in stabilizing a metastable BFO phase at this pressure.

Enlightening discussions with F. Petroff and V. Cros are gratefully acknowledged. This work has been supported by the EU STREP MACOMUFI (Contract No. 033221) and the contract FEMMES of the Agence Nationale pour la Recherche. H.B. also acknowledges financial support from the Conseil Général de l'Essonne.

*Electronic address: manuel.bibes@ief.u-psud.fr

†Present address: Physics Department, Trinity College, Dublin 2, Ireland.

[1] N. A. Hill, J. Phys. Chem. B **104**, 6694 (2000).

[2] G. A. Smolenskii and I. E. Chupis, Sov. Phys. Usp. **25**, 475 (1982).

[3] V. E. Wood and A. E. Austin, Int. J. Magn. **5**, 303 (1974).

[4] I. Žutić, J. Fabian, and S. Das Sarma, Rev. Mod. Phys. **76**, 323 (2004).

[5] M. Fiebig, J. Phys. D **38**, R123 (2005).

[6] Ch. Binek and B. Doudin, J. Phys.: Condens. Matter **17**, L39 (2005).

[7] Ch. Binek, A. Hochstrat, X. Chen, P. Borisov, W. Kleemann, and B. Doudin, J. Appl. Phys. **97**, 10C514 (2005).

[8] J. Wang, J. B. Neaton, H. Zheng, V. Nagarajan, S. B. Ogale, B. Liu, D. Viehland, V. Vaithyanathan, D. G. Schlom, U. V. Waghmare, N. A. Spaldin, K. M. Rabe, M. Wuttig, and R. Ramesh, Science **299**, 1719 (2003).

[9] H. Béa, M. Bibes, A. Barthélémy, K. Bouzehouane, A. Khodan, J.-P. Contour, S. Fusil, F. Wyczisk, A. Forget, D. Lebeugle, D. Colson, and M. Viret, Appl. Phys. Lett. **88**, 062502 (2005).

[10] W. Eerenstein, F. D. Morrison, J. Dho, M. G. Blamire, J. F. Scott, and N. D. Mathur, Science **307**, 1203a (2005).

[11] F. Bai, J. Wang, M. Wuttig, J. Li, N. Wang, A. P. Pyatakov, A. K. Zvezdin, L. E. Cross, and D. Viehland, Appl. Phys. Lett. **86**, 032511 (2005).

[12] C. P. Hunt, B. M. Moskowitz, and S. K. Banerjee, *Rock Physics and Phase Transitions, a Handbook of Physical Constants* (American Geophysical Union, Washington, D.C., 1995).

[13] C. Ederer and N. A. Spaldin, Phys. Rev. B **71**, 224103 (2005).

[14] J. M. D. Coey, Phys. Rev. Lett. **27**, 1140 (1971).

[15] S. Czekaj, F. Nolting, L. J. Heyderman, P. R. Willmott, and G. van der Laan, Phys. Rev. B **73**, 020401(R) (2006).

[16] P. Morrall, F. Schedin, G. S. Case, M. F. Thomas, E. Dudzik, G. van der Laan, and G. Thornton, Phys. Rev. B **67**, 214408 (2003).

[17] J. P. Crocombette, M. Pollak, F. Jollet, N. Thromat, and M. Gautier-Soyer, Phys. Rev. B **52**, 3143 (1995).

[18] S. Brice-Profeta, M.-A. Arrio, E. Tronc, N. Menguy, I. Letard, C. Cartier dit Moulin, M. Noguès, C. Chanéac, J.-P. Jolivet, and Ph. Sainctavit, J. Magn. Magn. Mater. **288**, 354 (2005).

[19] M. A. Novojilov, O. Y. Gorbenko, I. E. Graboy, A. R. Kaul, H. W. Zandbergen, N. A. Babushkina, and L. M. Belova, Appl. Phys. Lett. **76**, 2041 (2000).

[20] S. V. Samoylenkov, O. Y. Gorbenko, I. E. Graboy, A. R. Kaul, H. W. Zandbergen, and E. Connolly, Chem. Mater. **11**, 2417 (1999).